Available online at www.sciencedirect.com
ScienceDirect
Remote Sensing of Environment 105 (2006) 286–298
Remote Sensing of Environment
www.elsevier.com/locate/rse

Influence of landscape spatial heterogeneity on the non-linear estimation of leaf area index from moderate spatial resolution remote sensing data

S. Garrigues [a,*], D. Allard [b], F. Baret [c], M. Weiss [d]

[a] University of Maryland's Earth System Science Interdisciplinary Center, College Park, MD
[b] Biométrie, INRA, Avignon, France
[c] Climat Sol Environnement, INRA, Avignon, France
[d] Noveltis, Toulouse,France

Received 27 September 2005; received in revised form 7 July 2006; accepted 15 July 2006

Abstract

The monitoring of earth surface dynamic processes requires global observations of the structure and the functioning of vegetation. Moderate resolution sensors (with pixel size ranging from 250 m to 7 km) provide frequent estimates of biophysical variables to characterize vegetation such as the leaf area index (LAI). However, the computation of LAI from moderate resolution remote sensing data induces a scaling bias on the LAI estimate if the moderate resolution pixel is heterogeneous and if the transfer function that relates remote sensing data to LAI is non-linear.

This study provides a model to evaluate and correct the scaling bias. The model is built first for a univariate semi-empirical transfer function relating LAI directly to NDVI. The scaling bias is a function of (i) the degree of non-linearity of the transfer function quantified by its second derivative and (ii) the spatial heterogeneity of the moderate resolution pixel quantified by the variogram of the high spatial resolution (20 m) NDVI image. Then, the model is extended to a bivariate transfer function where LAI is related to red and near infrared reflectances. The scaling bias depends on (i) the Hessian matrix of the transfer function and (ii) the variograms and cross variogram of the red and near infrared reflectances.

The scaling bias is investigated on several distinct landscapes from the VALERI database. Adjusting for scaling bias is critical on crop sites which are the most heterogeneous sites at the landscape level. Regarding the univariate transfer function, the magnitude of the scaling bias increases rapidly with pixel size until this size is larger than the typical spatial scale of the data. For the bivariate transfer function, it results from the addition of several components that may add up or cancel each other out. It is thus more difficult to analyze.

The accuracy of the model to estimate the scaling bias is discussed. It depends mainly on the ability of the variograms and cross variogram to represent the local dispersion variances and covariance within the moderate resolution pixel. The model is generally highly accurate at 1000 m spatial resolution for the univariate transfer function and less accurate for the bivariate transfer function.

Keywords: Scaling bias; Spatial heterogeneity; Non-linearity; Leaf area index; Moderate resolution remote sensing data; Transfer function; Variogram; Dispersion variance

1. Introduction

Among the several components of the Earth system, processes related to the land surface are the most variable (Tian et al., 1998; Asner & Townsend, 2000). They are also poorly quantified at global scale (Houghton et al., 2001). The modeling of these processes requires state variables provided at the relevant spatial and temporal resolution either to force the model or to control its temporal trajectory with assimilation techniques (Cayrol et al., 2000). Among these state variables, the leaf area index (LAI), defined as half the total developed area of leaves per unit ground horizontal surface area (Chen & Black, 1992), characterizes the structure and the functioning of vegetation. It can be spatially estimated from remotely sensed radiance data using a transfer function derived either from a radiative transfer model (Weiss & Baret 1999) or from the calibration of a semi-empirical relationship (Sellers, 1987; Baret & Guyot, 1991). To resolve rapid changes of vegetation status and amount under both the influence of climate and human activities, relatively high revisit frequency observations are

* Corresponding author. NASA GSFC, Mail Code 614.4, Greenbelt, MD 20771, USA. Tel.: +1 301 6146646.
E-mail address: Sebastien.garrigues@gsfc.nasa.gov (S. Garrigues).

0034-4257/$ - see front matter © 2006 Elsevier Inc. All rights reserved.
doi:10.1016/j.rse.2006.07.013

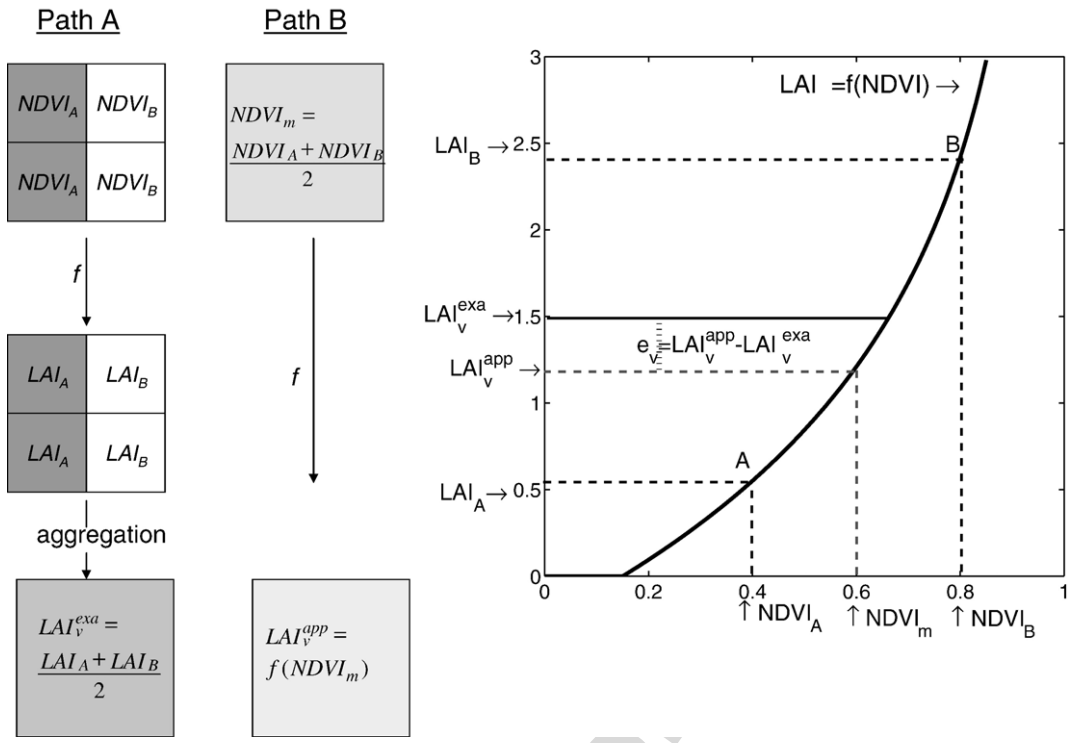

Fig. 1. Effect of the intra-pixel spatial heterogeneity on the non-linear estimation of LAI at moderate resolution. *f* is a semi-empirical transfer function relating LAI and NDVI. $NDVI_A$ and $NDVI_B$ are the high spatial resolution homogeneous NDVI data. LAI_A and LAI_B are their corresponding LAI values. LAI_v^{exa}, defined as the average between LAI_A and LAI_B, is the exact LAI value at the moderate resolution *v*. $NDVI_m$, defined as the average between $NDVI_A$ and $NDVI_B$, is the heterogeneous NDVI data at the moderate spatial resolution *v*. LAI_v^{app}, computed from the direct application of *f* to $NDVI_m$, is the approximated LAI at the resolution *v*. e_v, defined as the difference between LAI_v^{app} and LAI_v^{exa}, is the LAI scaling bias at the moderate resolution *v*.

required, currently provided by moderate resolution sensors with pixel size ranging from 250 m to 7 km (e.g. MODIS/TERRA-AQUA, MERIS/ENVISAT, VEGETATION/SPOT, POLDER/ADEOS-PARASOL).

LAI is a key player within a broad range of land surface models including vegetation (Moulin et al., 1998; Cayrol et al., 2000), biogeochemical (Running et al., 1999) or global atmospheric circulation models (Avissar & Chen, 1993). Improving and assessing the accuracy of LAI estimates is therefore required (Morisette et al., 2002, 2006; Baret et al., in press). Several sources of uncertainties degrade its estimation from remote sensing data (Hall et al., 1992; Friedl et al., 1995; Myneni et al., 1995; Dungan, 2002). The transfer function algorithm is associated with uncertainties originating from the calibration of the semi-empirical model, the assumptions related to the radiative transfer model and the inversion algorithm, or the applicability of the algorithm to a range of vegetation types, seasons and locations. Radiometric uncertainties attached to the radiance or reflectance measurement used as input in the transfer function are due to the sensor system, residual atmospheric effects or cloud contamination. Finally, the application at moderate resolution of a transfer function calibrated at high resolution induces a scaling bias on the LAI estimate if the transfer function is non-linear and the moderate resolution pixel is heterogeneous (Raffy, 1994; Friedl et al., 1995; Hu & Islam, 1997; Heuvelink & Pebesma, 1999; Lovejoy et al., 2001). This work focuses on the analysis of this last source of uncertainty.

The cause of the scaling bias is illustrated on a synthetic example of a semi-empirical transfer function between the normalized difference vegetation index (NDVI) and the LAI (Fig. 1). For the clarity of exposition, the non-linearity of the NDVI as a function of the near infrared and red reflectances is not taken into account in this demonstrating example. The transfer function *f* is calibrated at high spatial resolution (defined in this study as a pixel size of 20 m) at which the data ($NDVI_A$ and $NDVI_B$) are assumed to be homogeneous within each pixel. The exact value of the LAI (LAI_v^{exa}) at the moderate resolution *v* is obtained by first applying *f* at high spatial resolution and then by aggregating the result at the moderate resolution *v* (path A in Fig. 1). However, the direct application of *f* at the moderate resolution *v* (LAI_v^{app}) underestimates the exact LAI value (path B in Fig. 1) because of both the non-linearity of *f* and the spatial heterogeneity of the moderate resolution pixel.

The scaling bias is rarely taken into account in non-linear estimation processes of LAI at moderate spatial resolution despite the existence of sometimes large intra-pixel spatial herogeneity, especially in some agricultural landscapes (Garrigues et al., 2006). The scaling bias on LAI may reach up to 50% of the exact LAI value (Friedl, 1997; Chen, 1999; Weiss et al., 2000; Tian et al., 2002). To limit the influence of spatial heterogeneity on the non-linear estimation processes of LAI, a rational approach is to use a proper spatial resolution at which the variability of the landscape is captured by the sensor and the intra-pixel variability is minimized (Townshend & Justice,

Table 1
Database (detailed information on each site is available on the VALERI website www.avignon.inra.fr/valeri)

Site name	Biome (FAO classification)	Date	Latitude	Longitude	m_{NDVI}	σ_{NDVI}
Fundulea01	Cropland	May	44.41	26.58	0.51	0.23
Alpilles01	Cropland	March	43.81	4.74	0.41	0.19
Barrax03	Cropland	July	39.06	2.10	0.29	0.19
SudOuest02	Cropland	July	43.51	1.24	0.50	0.17
Alpilles02	Cropland	July	43.81	4.74	0.38	0.16
Gilching02	Cropland and mixed forest	July	48.08	11.33	0.60	0.12
Laprida01	Grassland	November	36.99	−60.55	0.62	0.09
Larzac01	Grassland	July	43.95	3.12	0.49	0.06
Jarvselja01	Mixed forest	July	58.29	27.29	0.82	0.05
Nezer01	Needleleaf forest (pine forest)	June	44.51	−1.04	0.66	0.06
Counami01	Broadleaf forest (tropical forest)	October	05.35	53.25	0.69	0.03
Puechabon01	Closed shrubland (Mediterranean vegetation)	June	43.72	3.65	0.54	0.10

Date is the acquisition month of the SPOT-HRV scene. m_{NDVI} and σ_{NDVI} are the mean and standard deviation of the NDVI image.

1988; Marceau et al., 1994; Garrigues et al., 2006). This will generally require relatively high spatial resolution observations for most landscapes (Garrigues et al., 2006). However, these observations are not currently acquired at a sufficiently high temporal frequency to resolve vegetation changes. In addition, most of the currently available LAI products are derived from moderate resolution data (Morisette et al., in press). While finer spatial resolution products associated with high temporal frequency should appear in the coming years, long time series of LAI covering past observations are mandatory for a range of applications (Myneni et al., 1997). The spatial heterogeneity has therefore to be explicitly taken into account in non-linear estimation processes.

Several authors have considered the problem of correcting the scaling bias. Assuming a uniform spatial distribution of the radiometric variables within the moderate resolution pixel, Raffy (1994) shows that the range of the possible values of LAI_v^{exact} is defined by the upper and lower limits of the transfer function convex hull. The scaling bias is then estimated as half of the amplitude of this range. This approach assumes that all possible values of LAI are equally likely and that the input variables within the pixels are uncorrelated. These assumptions are inappropriate to model the spatial distribution of the input variable within a moderate resolution pixel. They largely overestimate the actual spatial variability and lead to over-estimated scaling bias. An alternative method based on the disaggregation of moderate resolution pixels (Faivre & Fischer, 1997) consists in retrieving the radiometric values of several homogeneous patches constituting the pixel. This is generally achieved using a high spatial resolution land cover map. Faivre and Fischer (1997) showed that this method is appropriate on crop sites when applied over an important set of pixels and an updated high spatial resolution land cover map. In a third approach, a Taylor expansion of the transfer function is used to compute analytically the scaling bias as a function of the intra-pixel spatial heterogeneity and the degree of non-linearity of the transfer function (Hu & Islam, 1997; Chen, 1999; Pelgrum, 2000). The studies developing this approach differ in the metrics used to quantify the intra-pixel spatial heterogeneity. Most studies used an empirical metric of the spatial heterogeneity for each moderate resolution pixel. Garrigues et al. (2006) show that variogram modeling is an efficient method to characterize the loss of image spatial variability captured by the sensor as its spatial resolution decreases. The variogram of high spatial resolution data can therefore be used to quantify explicitly the mean spatial heterogeneity within the moderate spatial resolution pixels covering the same area as the high spatial resolution image. In this paper, an approach based on variogram modeling of high spatial resolution radiometric data is developed to correct the scaling bias. Since variogram modeling may be applied to several variables, this approach may be extended to estimate the scaling bias associated with a multivariate transfer function.

Several authors have reported that the magnitude of the scaling bias increases with both the degree of non-linearity of the model and the heterogeneity of the input surface (Raffy, 1994; Friedl, 1997; Hu & Islam, 1997; Chen, 1999). In these studies, the scaling bias was investigated either on simulated landscape images or on a limited number of land cover types. In this paper, the scaling bias associated with the non-linear relationship between NDVI and LAI is quantified over several types of landscape. In addition, few studies have analyzed how the scaling bias propagates through the composition of several non-linear models. This issue will be specifically addressed in this paper.

The VALERI database (Validation of Land European Remote sensing Instruments), presented in the second section, is used to investigate the scaling bias associated with the non-linear estimation process of LAI over several types of landscapes. The third section provides the theoretical framework to estimate the scaling bias: the model is first built for a semi-empirical transfer function relating directly LAI to NDVI; then generalized to a bivariate transfer function where LAI is directly derived from red and near infrared reflectances. In Section 4, the magnitude of the scaling bias is related to the spatial heterogeneity characteristics of the landscapes and the propagation mechanisms generating the LAI scaling bias when LAI is derived from the red and near infrared reflectances are analyzed. In Section 5, the accuracy of the proposed correction of the LAI scaling bias is assessed on the VALERI database in the univariate and bivariate case.

2. Description of the data

The data used here are part of the VALERI database which provides high spatial resolution (20 m) SPOT-HRV scenes for several landscapes sampled through the world (Baret et al., in press). The red (0.61–0.67 μm), denoted $r(x)$, and near infrared (0.78–0.89 μm), denoted $p(x)$, reflectances are derived from the SPOT-HRV data. For each 20 m pixel x, an NDVI value, denoted $z(x)$, is computed according to the function $g_{p,r}$:

$$g_{p,r} : z(x) = \frac{p(x) - r(x)}{p(x) + r(x)} \tag{1}$$

The scenes are georeferenced in the UTM/WGS84 projection. They are not contaminated by clouds except in the tropical forest image for which a cloud mask was applied. They are not corrected for atmospheric scattering and absorption. But, for most scenes, the atmospheric effects are low in the red and near-infrared bands (Baret et al., in press).

For this study, 12 sites with distinct landscape spatial heterogeneity (Table 1) were selected. The sites have flat topography, a standard size of 3000 m * 3000 m and they contain one or two types of vegetation.

To generate the LAI map on each site, a semi-empirical transfer function f (Eq. (2), Baret and Guyot, 1991) is applied to the high spatial resolution NDVI image:

$$f : \ \mathrm{LAI} = \frac{-1}{K_{\mathrm{NDVI}}} \log\left(\frac{z(x) - \mathrm{NDVI}_\infty}{\mathrm{NDVI}_s - \mathrm{NDVI}_\infty}\right) \tag{2}$$

The extinction coefficient K_{NDVI} and the asymptotic value NDVI_∞ are estimated from several simulations of a radiative transfer model (SAIL, Verhoef, 1984) that accounts for a broad range of canopy architectures (Weiss et al., 2002). The NDVI soil value NDVI_s is computed empirically on each site by averaging the NDVI value of pixels identified as bare soil. The NDVI values are assumed to be within the interval $[\mathrm{NDVI}_s, \mathrm{NDVI}_\infty[$ on which f is continuous and differentiable. The LAI computed from the transfer function f is defined assuming a random spatial distribution of the vegetation elements in agreement with the radiative transfer model on which f was established. In this paper, the transfer function f is used specifically to investigate the scaling bias at moderate spatial resolution. Therefore, its accuracy to estimate the LAI will not be discussed here.

Although there is still some possible spatial variability within the high spatial resolution pixel, this will not be considered because it was not accessible. The transfer function f is therefore assumed to be without any scaling bias at 20 m spatial resolution.

3. Scaling bias modeling

3.1. Univariate model

High spatial resolution NDVI data are aggregated to coarser resolutions v (60 m, 100 m, 200 m, 300 m, 500 m, 1000 m) using a perfect rectangular point spread function (Eq. (3)). The scaling bias caused by the non-linearity of the NDVI as a function of the near infrared and red reflectances is not considered in this univariate model, but will be the subject of the next section. This amounts to computing the NDVI of the moderate resolution pixel v as the simple average of the n high spatial resolution NDVI values $z(x_\alpha)$,

$$z_v = \frac{1}{n}\sum_{\alpha=1}^{n} z(x_\alpha), \tag{3}$$

where z_v is the aggregated NDVI value at the moderate resolution v and n is the number of high resolution pixels within v. As explained in the Introduction, the application of f at moderate resolution leads to an approximated LAI value $\mathrm{LAI}_v^{\mathrm{app}}$:

$$\mathrm{LAI}_v^{\mathrm{app}} = f(z_v) \tag{4}$$

The exact LAI value $\mathrm{LAI}_v^{\mathrm{exa}}$ is computed by first applying f at high spatial resolution and then by aggregating the result at the moderate resolution v:

$$\mathrm{LAI}_v^{\mathrm{exa}} = \frac{1}{n}\sum_{\alpha=1}^{n} f(z(x_\alpha)) \tag{5}$$

The difference between $\mathrm{LAI}_v^{\mathrm{app}}$ and $\mathrm{LAI}_v^{\mathrm{exa}}$ is the univariate scaling bias e_v:

$$e_v = f(z_v) - \frac{1}{n}\sum_{\alpha=1}^{n} f(z(x_\alpha)) \tag{6}$$

We propose a model, based on the approach developed by Hu and Islam (1997), to estimate this scaling bias. Assuming that $z(x)$ varies slowly within v, the scaling bias e_v is approximated by a second order Taylor development of f around z_v:

$$e_v \approx -\frac{1}{n}\sum_{\alpha=1}^{n} f'(z_v)(z(x_\alpha) - z_v) - \frac{1}{n}\sum_{\alpha=1}^{n} \frac{f''(z_v)}{2}(z(x_\alpha) - z_v)^2 \tag{7}$$

In Eq. (7),

$$\frac{1}{n}\sum_{\alpha=1}^{n} f'(z_v)(z(x_\alpha) - z_v) = f'(z_v)\left(\frac{1}{n}\sum_{\alpha=1}^{n}(z(x_\alpha) - z_v)\right) = 0 \tag{8}$$

and

$$\frac{1}{n}\sum_{\alpha=1}^{n}(z(x_\alpha) - z_v)^2 = s^2_{loc}(x|v) \tag{9}$$

is the local dispersion variance which quantifies the spatial variability of $z(x)$ within v (Garrigues et al., 2006). The scaling bias e_v, is thus approximated by Eq. (10):

$$e_v \approx -\frac{f''(z_v)}{2} s^2_{loc}(x|v) \tag{10}$$

Therefore, it depends on two multiplicative factors: (i) the degree of non-linearity of the transfer function at z_v, characterized by $f''(z_v)$, and (ii) the local spatial heterogeneity of the NDVI

within the moderate resolution pixel given by $s^2_{\mathrm{loc}}(x|v)$. Therefore, e_v is null either when f is linear or when the moderate resolution pixel is homogeneous. It is negative for a convex function such as the transfer function f in Eq. (2). Since $s^2_{\mathrm{loc}}(x|v)$ is generally not known at moderate resolution (unless a simultaneous high spatial resolution image is available), *a priori* information about the intra-pixel spatial heterogeneity is required to estimate the scaling bias.

In the framework of second order stationary random functions (Chilès & Delfiner, 1999; Wackernagel, 2003), $z(x)$ is considered as a realization of a (second order stationary) random function, $Z(x)$. The variogram, denoted $\gamma(h)$, of $Z(x)$ describes the variability between two pixel values separated by a distance h:

$$\gamma(h) = 0.5Var[Z(x+h) - Z(x)] \tag{11}$$

In this framework, $s^2_{loc}(x|v)$, e_v, and z_v are realizations of random variables, respectively denoted $S^2_{loc}(x|v)$, E_v, and Z_v. We define the theoretical scaling bias $e_{v,\mathrm{th}}$ as the mathematical expectation of E_v conditional to Z_v:

$$\begin{aligned} e_{v,\mathrm{th}} &= E[E_v|Z_v] = -\frac{f''(Z_v)}{2} E\left[S^2_{loc}(x|v)\right] \\ &= -\frac{f''(Z_v)}{2}\gamma(v,v) \end{aligned} \tag{12}$$

In Eq. (12), $\gamma(v,v)$ is the theoretical dispersion variance of $Z(x)$ within the domain v (Chilès & Delfiner, 1999; Garrigues et al., 2006). It is defined as the mathematical expectation of the local dispersion variance $S^2_{loc}(x|v)$ and is equal to

$$\gamma(v,v) = \frac{1}{|v|^2}\int_{x\in v}\int_{y\in v}\gamma(|x-y|)dxdy \tag{13}$$

where $|x-y|$ represents the distance between the points x and y within the domain v. It can easily be computed once a model of variogram has been fitted to the experimental variogram computed on the high spatial resolution image. It quantifies the mean spatial heterogeneity within the moderate spatial resolution pixels v covering the same area than the high spatial resolution image. Note that $\gamma(v,v)$ can also be interpreted as the loss of image variability when aggregating the high spatial resolution pixels to the moderate spatial resolution v.

The corrected $\mathrm{LAI}^{\mathrm{corr}}_v$ at moderate spatial resolution is computed by Eq. (14).

$$\mathrm{LAI}^{\mathrm{corr}}_v = \mathrm{LAI}^{\mathrm{app}}_v - e_{v,\mathrm{th}} \tag{14}$$

To assess the accuracy of this correction, we use the relative gain of the root mean square error (RMSE), $RRMSE_v$:

$$\mathrm{RRMSE}_v = \frac{\mathrm{RMSE}^{\mathrm{app}}_v - \mathrm{RMSE}^{\mathrm{corr}}_v}{\mathrm{RMSE}^{\mathrm{app}}_v}, \tag{15}$$

where $\mathrm{RMSE}^{\mathrm{app}}_v$ and $\mathrm{RMSE}^{\mathrm{corr}}_v$ are the RMSE of the $\mathrm{LAI}^{\mathrm{app}}_v$ and the $\mathrm{LAI}^{\mathrm{corr}}_v$ relative to $\mathrm{LAI}^{\mathrm{exa}}_v$, respectively.

3.2. Bivariate model

The previous model developed for a transfer function of a single radiometric variable (NDVI) may be extended to a multivariate transfer function. In this work, we provide the model for a bivariate transfer function but generalization to more than two variables is direct. Replacing the NDVI by its formula (Eq. (1)) in the function f (Eq. (2)), we define the bivariate transfer function $f_{p,r}$:

$$f_{p,r} : \mathrm{LAI} = \frac{-1}{K_{\mathrm{NDVI}}}\log\left(\frac{\frac{p(x)-r(x)}{p(x)+r(x)} - \mathrm{NDVI}_\infty}{\mathrm{NDVI}_s - \mathrm{NDVI}_\infty}\right) \tag{16}$$

We assume that the parameters NDVI_s and NDVI_∞ are such that:

$$\mathrm{NDVI}_s \le \frac{p(x)-r(x)}{p(x)+r(x)} < \mathrm{NDVI}_\infty \tag{17}$$

As a result, $f_{p,r}$ is continuous and differentiable for both variables p and r. Let us denote $e_{v,biva}$ the bivariate scaling bias between $\mathrm{LAI}^{\mathrm{app}}_{v,\mathrm{biva}}$, estimated using the moderate resolution red and near infrared reflectances, and $\mathrm{LAI}^{\mathrm{exa}}_v$,

$$e_{v,biva} = f_{p,r}(p_v, r_v) - \frac{1}{n}\sum_{\alpha=1}^{n} f_{p,r}(p(x_\alpha), r(x_\alpha)) \tag{18}$$

where p_v and r_v are the variables p and r aggregated at the moderate resolution v.

The scaling bias $e_{v,biva}$ is approximated by a second order Taylor development of $f_{p,r}$ around the vector of variables (p_v, r_v). Then, using the same arguments than in the univariate case, the bivariate scaling bias is approximated by:

$$\begin{aligned} e_{v,biva} \approx -0.5\Bigg[&\frac{\partial^2 f_{p,r}}{\partial p^2}(p_v, r_v)s^2_{loc,p}(x|v) + \frac{\partial^2 f_{p,r}}{\partial r^2}(p_v, r_v)s^2_{loc,r}(x|v) \\ &+2\frac{\partial^2 f_{p,r}}{\partial p \partial r}(p_v, r_v)c_{loc,p,r}(x|v)\Bigg] \end{aligned} \tag{19}$$

In Eq. (19), $\frac{\partial^2 f_{p,r}}{\partial p^2}$, $\frac{\partial^2 f_{p,r}}{\partial r^2}$, and $\frac{\partial^2 f_{p,r}}{\partial p \partial r}$ are the components of the Hessian matrix of the bivariate function $f_{p,r}$. For the transfer function considered in (16), $\frac{\partial^2 f_{p,r}}{\partial p^2}(p_v, r_v)$ is negative, $\frac{\partial^2 f_{p,r}}{\partial r^2}(p_v, r_v)$ is positive and $\frac{\partial^2 f_{p,r}}{\partial p \partial r}(p_v, r_v)$ is negative. As in Eq. (10), $s^2_{loc,p}(x|v)$ and $s^2_{loc,r}(x|v)$ are the local dispersion variances of the high spatial resolution variables p and r, respectively. In the multivariate approach, it is also necessary to define the local dispersion covariance between the high spatial resolution variables p and r, $c_{loc,p,r}(x|v)$:

$$c_{loc,p,r}(x|v) = \frac{1}{n}\sum_{\alpha=1}^{n}(p(x_\alpha) - p_v)(r(x_\alpha) - r_v) \tag{20}$$

It quantifies the spatial co-variability between the high spatial resolution variables p and r within the moderate resolution pixel v.

Contrary to the scaling bias of the univariate transfer function f, the sign of the bivariate scaling bias $\mathrm{e}_{v,\mathrm{biva}}$ may not be constant. It is the result of the interaction between the Hessian matrix components of $f_{p,r}$ and the dispersion variances and covariance of the near infrared and red variables.

An estimator of the empirical bias is then built in the framework of second order stationary random functions. The theoretical scaling bias $e_{v,\mathrm{biva,th}}$ is defined as the mathematical expectation of the scaling bias random variable $E_{v,biva}$ conditional to the vector of random variables (P_v, R_v),

$$\begin{aligned} e_{v,\mathrm{biva,th}} &= E\lfloor E_{v,\mathrm{biva}} | (P_v, R_v) \rfloor \\ &= -0.5\left[\frac{\partial^2 f_{p,r}}{\partial p^2}(P_v,R_v)\gamma_p(v,v) + \frac{\partial^2 f_{p,r}}{\partial r^2}(P_v,R_v)\gamma_r(v,v) \right. \\ &\quad \left. +2\frac{\partial^2 f_{p,r}}{\partial p \partial r}(P_v,R_v)\gamma_{p,r}(v,v)\right] \end{aligned} \quad (21)$$

where $\gamma_p(v,v)$ and $\gamma_r(v,v)$ are the theoretical dispersion variances of the variables p and r and $\gamma_{p,r}(v,v)$ is the theoretical dispersion covariance between p and r. They are computed from the double integration (Eq. (13)) of the corresponding variograms and cross variogram modeled together using the widely used linear coregionalization model (Wackernagel, 2003).

4. Analysis of the scaling bias

In this section, the factors acting on the scaling bias are analyzed in the light of the analytical model provided previously.

4.1. Univariate scaling bias

The sign of the scaling bias e_v associated with the transfer function f is constant and negative (Section 3.1, Eq. (12)). In the following, we evaluate its magnitude relative to $\mathrm{LAI}_v^{\mathrm{exa}}$

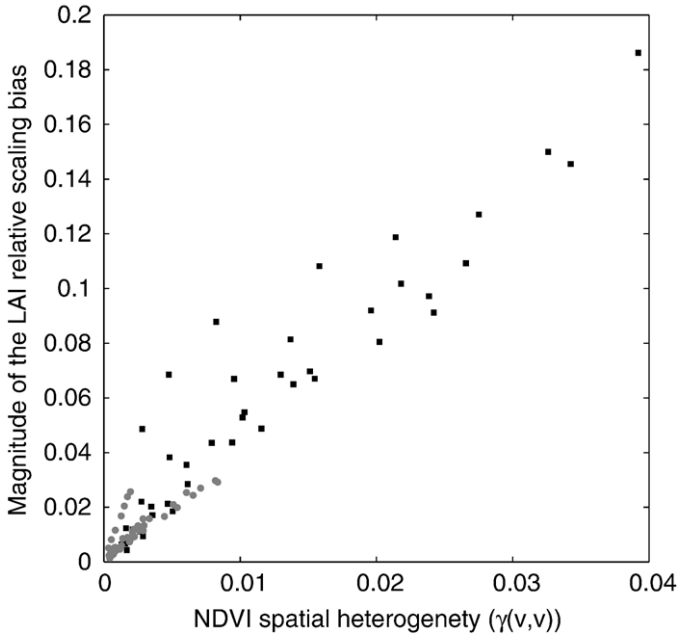

Fig. 2. Average of the magnitude of the univariate scaling bias relative to $\mathrm{LAI}_v^{\mathrm{exa}}(|\overline{e_v^{\mathrm{rel}}}|)$ over each site as a function of the NDVI spatial heterogeneity $\gamma(v, v)$ within the moderate resolution pixel v for several spatial resolutions (60 m, 100 m, 300 m, 500 m, 1000 m). The gray circles are natural and forest homogeneous sites. The black squares represent heterogeneous cropland sites.

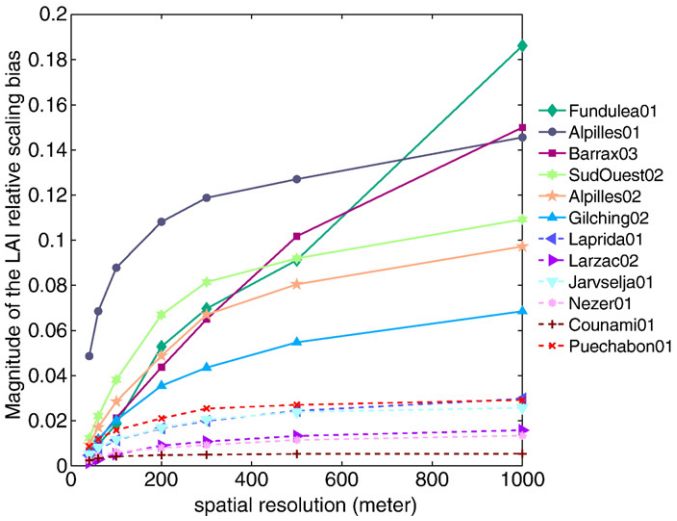

Fig. 3. Average of the magnitude of the univariate scaling bias relative to $\mathrm{LAI}_v^{\mathrm{exa}}(|\overline{e_v^{\mathrm{rel}}}|)$ over each site as a function of spatial resolution v. The solid lines are cropland and the dashed lines are natural and forest vegetation sites.

quantified on each landscape and at a given spatial resolution v by its average over the scene (Figs. 2 and 3):

$$|\overline{e_v^{\mathrm{rel}}}| = \frac{1}{P}\sum_{i=1}^{P}\frac{|e_{v_i}|}{\mathrm{LAI}_{v_i}^{exa}} \quad (22)$$

where P is the number of pixels v_i covering the scene and e_{vi} is the scaling bias of the pixel v_i.

The magnitude of the scaling bias is proportional to the intra-pixel spatial heterogeneity quantified by the theoretical dispersion variance $\gamma(v,v)$ (Fig. 2), which increases with the size of the pixel (Garrigues et al., 2006). As a result, the LAI scaling bias is higher at 1000 m spatial resolution (Fig. 3, maximum relative bias of 19%) than at 500 m spatial resolution (Fig. 3, maximum relative bias of 12%).

The dispersion variance $\gamma(v,v)$ is an increasing function of the landscape spatial variability (Garrigues et al., 2006). In the VALERI database, crop sites are more heterogeneous than natural vegetation and forest sites at the landscape level (Fig. 2). Consequently, the magnitude of the LAI scaling bias is larger on crop sites (Fig. 3, relative bias between 10% and 19% at 1000 m spatial resolution) than on natural vegetation sites (Fig. 3, relative bias between 0.5% and 3% at 1000 m spatial resolution).

At a given spatial resolution, the dispersion variance depends also on the ratio between the pixel size and the length scales of the data, i.e. the extent of the spatial structures (i.e. patches) exhibited by the image (Garrigues et al., 2006). When the size of the moderate resolution pixel v is larger than the extent of the spatial structure, the spatial variability related to that spatial structure is not captured by the sensor, thus increasing the spatial heterogeneity within v. For example, at 500 m spatial resolution, the length scale of Fundulea01 (781 m) is still detected in the image, while on Alpilles01 an important spatial variability related to its smaller length scale (268 m) is lost (Garrigues et al., 2006). For this reason, the magnitude of the scaling bias is lower on Fundulea01 than on Alpilles01 at 500 m spatial resolution (Fig. 3).

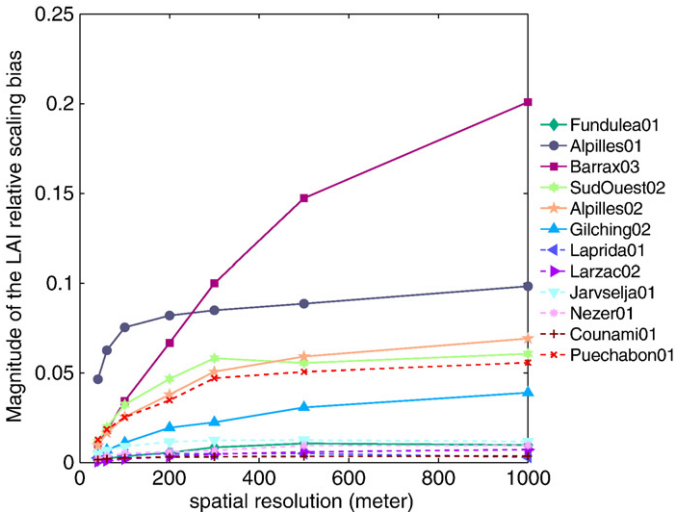

Fig. 4. Average of the magnitude of the bivariate scaling bias relative to $LAI_v^{exa}(|\overline{e_{v,biva}^{rel}}|)$ over each site as a function of the spatial resolution. The solid lines are cropland and the dashed lines are natural and forest vegetation sites.

But it increases considerably at 1000 m spatial resolution at which the Fundulea01 length scale, associated with a larger spatial variability than Alpilles01, is no longer captured in the image.

The magnitude of the scaling bias increases also with the degree of non-linearity of the transfer function f (Eq. (12)) which is an increasing function of the NDVI. Hence, the magnitude of the scaling bias increases with the NDVI value. For example, the Jarvselja01 mixed forest site shows large NDVI values (between 0.6 and 0.9 with a mean NDVI equal to 0.82, Table 1). Consequently, its scaling bias magnitude is close to that of Puechabon01 (Fig. 3) despite its low NDVI dispersion variance compared to the NDVI dispersion variance of Puechabon01. However, although most of the forest sites have large NDVI values, the magnitude of their scaling bias is low because they are homogeneous (small values of $\gamma(v,v)$, Fig. 2). On cropland sites, the range of NDVI values is larger (between 0.2 and 0.8 on Fundulea01). Hence, on heterogeneous pixels with low NDVI values (bare soil field), the low degree of non-linearity limits the magnitude of the scaling bias while on heterogeneous pixels with high NDVI values (vegetation field) the high degree of non-linearity increases the magnitude of the scaling bias.

As a conclusion, the magnitude of the scaling bias is large on crop sites which are the most heterogeneous sites at the landscape level. It increases rapidly with pixel size until this size is larger than the typical length scale of the data, i.e. between 250 m and 1000 m spatial resolution for the cropland sites under study. Since it is amplified by the degree of non-linearity of the transfer function, it may change according to the type of transfer function used. Finally, the spatial heterogeneity and the NDVI values depend on the phenological state of the vegetation. As a result, the magnitude of the scaling bias will also vary seasonally.

4.2. Bivariate scaling bias

The sign of the scaling bias $e_{v,biva}$ associated with the transfer function $f_{p,r}$ may be non-constant (Section 3.2, Eq. (21)). In the

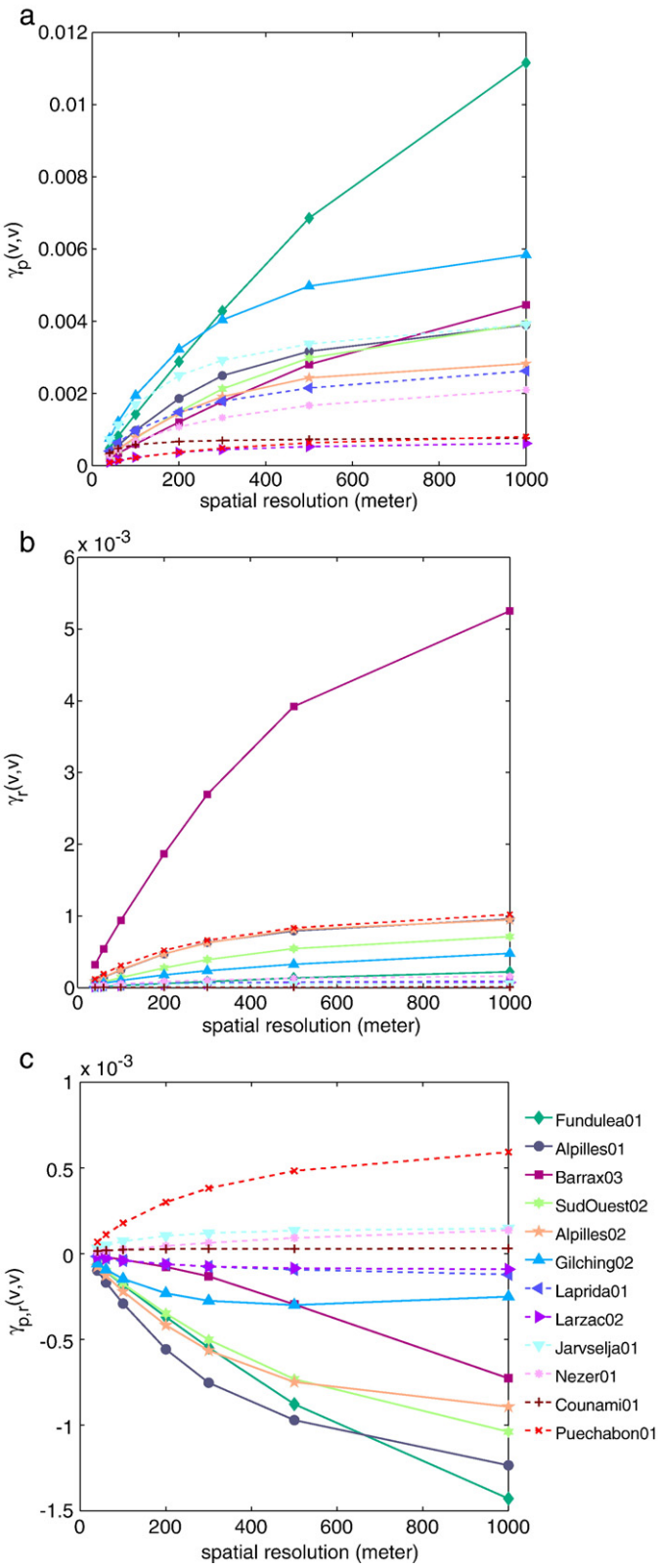

Fig. 5. Characterization of the spatial heterogeneity of the near infrared and red reflectances at moderate spatial resolution: (a) Dispersion variance of the near infrared $\gamma_p(v,v)$ versus spatial resolution. (b) Dispersion variance of the red $\gamma_r(v,v)$ versus spatial resolution. (c) Dispersion covariance $\gamma_{p,r}(v,v)$ between the near infrared and the red versus spatial resolution.

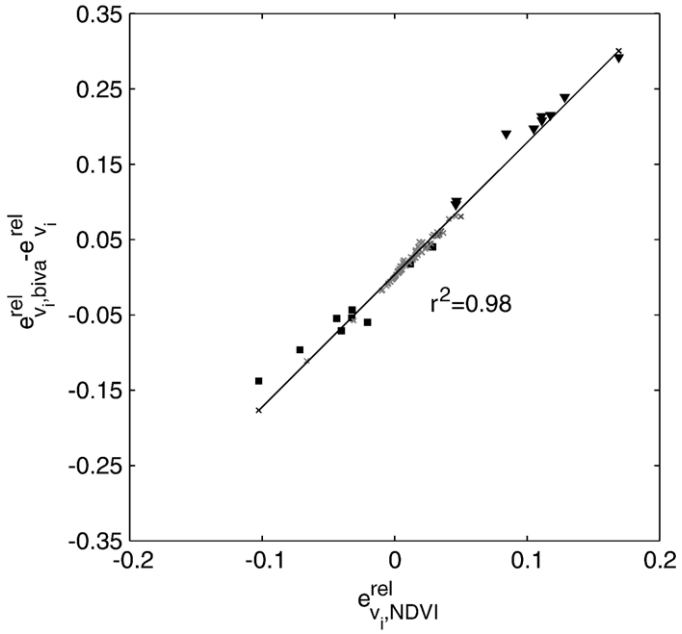

Fig. 6. Difference between the relative bivariate scaling bias $e^{rel}_{vi,biva}$ and the relative univariate scaling bias e^{rel}_{vi} as a function of the relative NDVI scaling bias $e^{rel}_{vi,NDVI}$ for each 1000 m spatial resolution moderate resolution pixel of each site. The black triangles represent the Fundulea01 site. The black squares represent the Barrax03 site. The gray crosses are the other sites.

following, we evaluate its magnitude relative to LAI^{exa}_{v} quantified on each landscape and at a given spatial resolution v by its average over the scene (Fig. 4):

$$\overline{|e^{rel}_{v,biva}|} = \frac{1}{P}\sum_{i=1}^{P}\frac{|e_{vi,biva}|}{LAI^{exa}_{v_i}} \quad (23)$$

where P is the number of pixels v_i covering the scene and $e_{vi,biva}$ is the bivariate scaling bias of the pixel v_i.

The magnitude of the scaling bias associated with the bivariate transfer function $f_{p,r}$ is generally larger on crop sites than on natural and forest sites (Fig. 4), in agreement with results obtained with the univariate transfer function f. It increases with the pixel size and it is mainly explained by the values of the dispersion variances and dispersion covariance of the red and near infrared variables (Fig. 5). However, on some landscapes, it is different than the scaling bias associated with the univariate transfer function. Since the description of spatial heterogeneity depends on the nature of the underlying radiometric variables, the dispersion variances of the red and near infrared variables are different than the NDVI dispersion variance. For example, on Barrax03, the red reflectance is very variable over the large bare soil area since it is sensitive to the soil properties while the NDVI is not. As a result, the dispersion variance of the red, $\gamma_r(v,v)$, increases the magnitude of the bivariate scaling bias compared to the magnitude of the univariate scaling bias. Besides, the bivariate scaling bias results from the sum of several terms which may add up or compensate for one another (Eq. (21)). On Fundulea01, the mosaic of vegetation fields with high NDVI values and bare soil fields with low NDVI values explains the high variability of the near infrared $\gamma_p(v,v)$ and the high dispersion covariance between red and near infrared $\gamma_{p,r}(v,v)$. The resulting magnitude of the scaling bias is low since $\gamma_p(v,v)$ is positive and associated with the negative term $\frac{\partial^2 f_{p,r}}{\partial p^2}(P_v, R_v)$ that compensates for the effect of $\gamma_{p,r}(v,v)$, which is negative and related to the negative term $\frac{\partial^2 f_{p,r}}{\partial p \partial r}(P_v, R_v)$. Conversely, on Alpilles01, the dispersion variance of the near infrared is lower than that of Fundulea01, while their dispersion covariances $\gamma_{p,r}(v,v)$ are similar. As a result, the magnitude of the bivariate scaling bias is higher on Alpilles01 than on Fundulea01.

In contrast to the univariate transfer function, the analysis of the magnitude of the scaling bias is more complex for a bivariate transfer function. It is the result of the interaction between the Hessian matrix components and the dispersion variances and covariance of the near infrared and red variables. The next section provides a further exploration of the differences between the univariate scaling bias and the bivariate scaling bias.

4.3. Propagation bias mechanisms

As mentioned in the previous section, the scaling bias of the univariate transfer function f and the scaling bias of the bivariate transfer function $f_{p,r}$ may show important discrepancies (Fig. 6). For most of the sites, the magnitude of the bivariate scaling bias is lower than the univariate one (e.g. difference up to 20% on Fundulea01 at 1000 m spatial resolution), but for some sites, like Barrax03 or Puechabon01, it is higher. At high spatial resolution, the functions f and $f_{p,r}$ are equivalent and the aggregated result leads to the same value of the LAI^{exa}_{v}. However, their application at moderate spatial resolution does not lead to the same LAI^{app}_{v} value. The NDVI is a non-linear function of the near infrared and red reflectances. When the moderate resolution pixel is heterogeneous, the NDVI aggregated at moderate resolution which is the input of the function f (left-hand side of Eq. (24)) differs from the NDVI computed from the aggregated near infrared and red reflectances which is the input of the function $f_{p,r}$ (right-hand side of Eq. (24)):

$$\frac{1}{n}\sum_{\alpha=1}^{n}\frac{p(x_\alpha)-r(x_\alpha)}{p(x_\alpha)+r(x_\alpha)} \neq \frac{p_v - r_v}{p_v + r_v} \quad (24)$$

To understand the differences between the univariate scaling bias associated with f and the bivariate scaling bias associated with $f_{p,r}$, we define $f_{p,r}$ as the compositing function of (Eq. (2)) f and $g_{p,r}$ (Eq. (1)):

$$f_{p,r} = f \circ g_{p,r} \quad (25)$$

Because of their non-linearity, both f and $g_{p,r}$ engender a scaling bias.

The difference between

$$NDVI^{exa}_{v} = \frac{1}{n}\sum_{\alpha=1}^{n}\frac{p(x_\alpha)-r(x_\alpha)}{p(x_\alpha)+r(x_\alpha)} \quad (26)$$

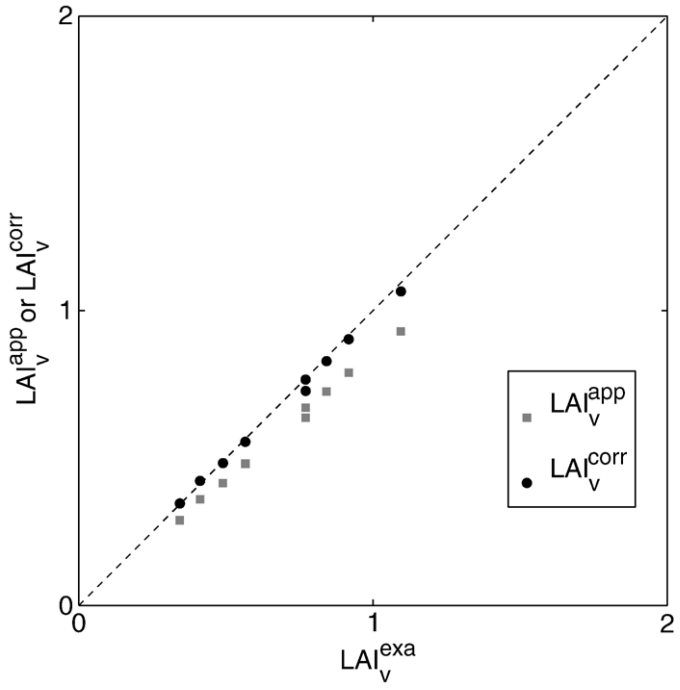

Fig. 7. Correction of the univariate scaling bias on Alpilles01 site (cropland) at $v=1000$ m spatial resolution. $\mathrm{LAI}_v^{\mathrm{exa}}$ is the exact LAI; $\mathrm{LAI}_v^{\mathrm{app}}$ is the approximated LAI before correction; $\mathrm{LAI}_v^{\mathrm{corr}}$ is the corrected LAI.

and

$$\mathrm{NDVI}_v^{\mathrm{app}} = \frac{p_v - r_v}{p_v + r_v} \tag{27}$$

is the NDVI scaling bias, denoted $e_{v,\mathrm{ndvi}}$. Its sign and its magnitude depend on the dispersion variances and dispersion covariance of the near infrared and red variables and on the Hessian matrix components of $g_{p,r}$ (Eq. (21) applied to $g_{p,r}$). For the function $g_{p,r}$, $\frac{\partial^2 g_{p,r}}{\partial r^2}(p_v, r_v)$ and $\frac{\partial^2 g_{p,r}}{\partial p \partial r}$ are positive, while $\frac{\partial^2 g_{p,r}}{\partial p^2}(p_v, r_v)$ is negative. Therefore, on Barrax03, the high value of $\gamma_r(v,v)$ generates a negative NDVI scaling bias. In contrast, on Fundulea01, the high value of $\gamma_p(v,v)$ and the high negative value of $\gamma_{p,r}(v,v)$ lead to a positive NDVI scaling bias. As shown in the x-axis of Fig. 6, the magnitude of the NDVI scaling bias is low (for most of the sites it is less than 4%) compared to the magnitude of the LAI scaling bias (Fig. 3). This

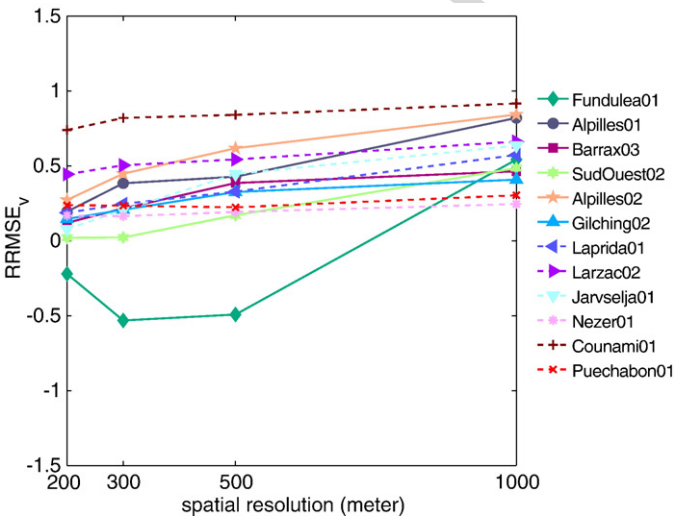

Fig. 8. Relative gain of the RMSE (RRMSE_v) associated with the univariate model for each site at 200 m, 300 m, 500 m, and 1000 m spatial resolution.

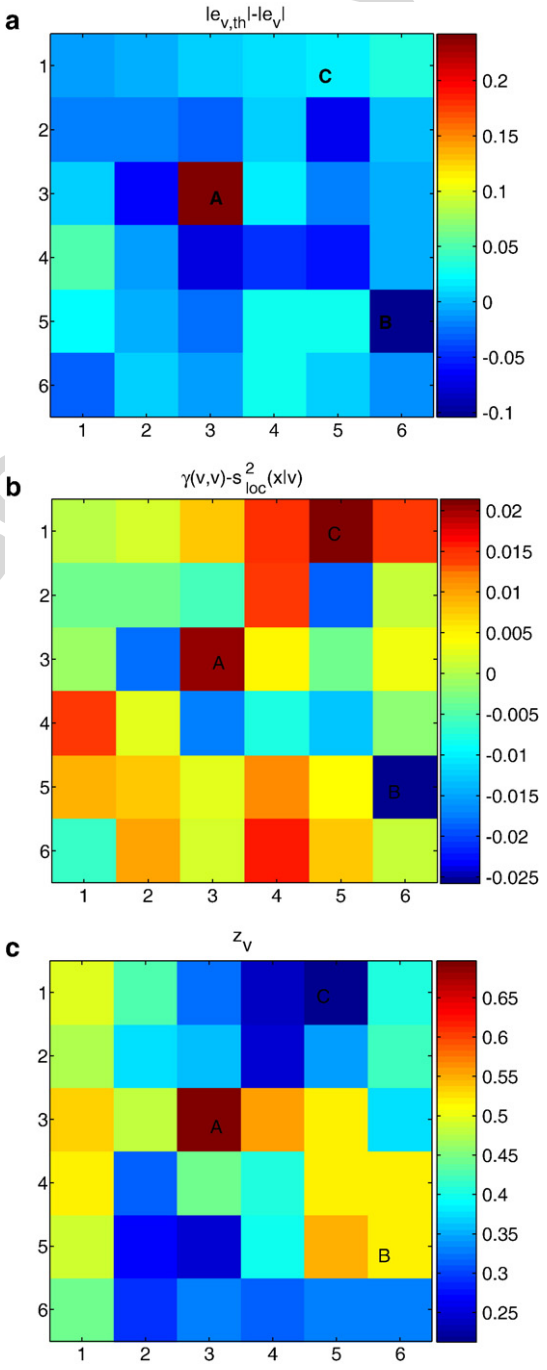

Fig. 9. Local estimation of the univariate scaling bias over each 500 m moderate resolution pixel of the Alpilles01 scene (cropland). (a) Difference between the magnitude of the estimated scaling bias $|e_{v,\mathrm{th}}|$ and the magnitude of the local bias $|e_v|$. (b) Difference between the theoretical dispersion variance $\gamma(v,v)$ and the local dispersion variance $s^2_{loc}(x|v)$ of the NDVI. (c) NDVI image at 500 m spatial resolution (indicator of the degree of non-linearity of the transfer function f).

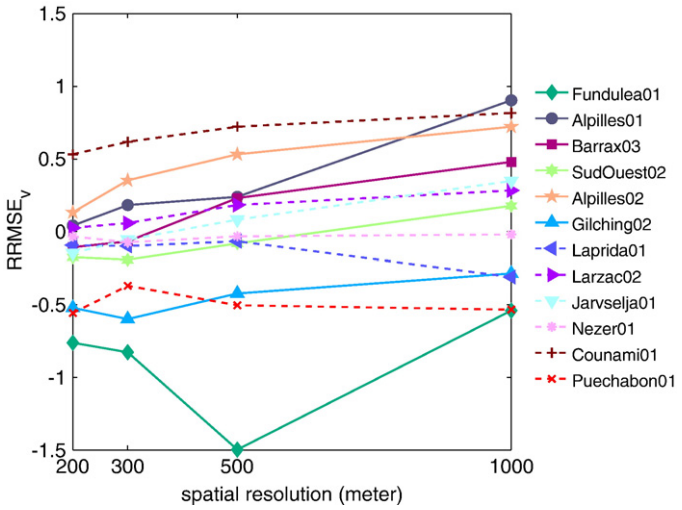

Fig. 10. Relative gain of the RMSE (RRMSE$_v$) associated with the bivariate model for each site at 200 m, 300 m, 500 m, and 1000 m spatial resolution.

is due to the lower degree of non-linearity of the function $g_{p,r}$ than that of the function f.

As mentioned in Section 4.1, the univariate scaling bias e_v related only to the non-linearity between LAI and NDVI (function f) is negative and its magnitude depends on both the dispersion variance of the NDVI and the second derivative of f.

The relationships between the bias $e_{v,\mathrm{biva}}$, e_v, and $e_{v,\mathrm{ndvi}}$ are investigated empirically. We define the relative values of $e_{v,\mathrm{biva}}$ and e_v to the exact LAI value (Eqs. (28) and (29)) and the relative value of $e_{v,\mathrm{ndvi}}$ to the exact NDVI value (Eq. (30))

$$e_v^{\mathrm{rel}} = \frac{e_v}{\mathrm{LAI}_v^{\mathrm{exa}}} \tag{28}$$

$$e_{v,\mathrm{biva}}^{\mathrm{rel}} = \frac{e_{v,\mathrm{biva}}}{\mathrm{LAI}_v^{\mathrm{exa}}} \tag{29}$$

$$e_{v,\mathrm{ndvi}}^{\mathrm{rel}} = \frac{e_{v,\mathrm{ndvi}}}{\mathrm{NDVI}_v^{\mathrm{exa}}} \tag{30}$$

As shown in Fig. 6, the differences between the relative bivariate scaling bias and the relative univariate scaling bias are

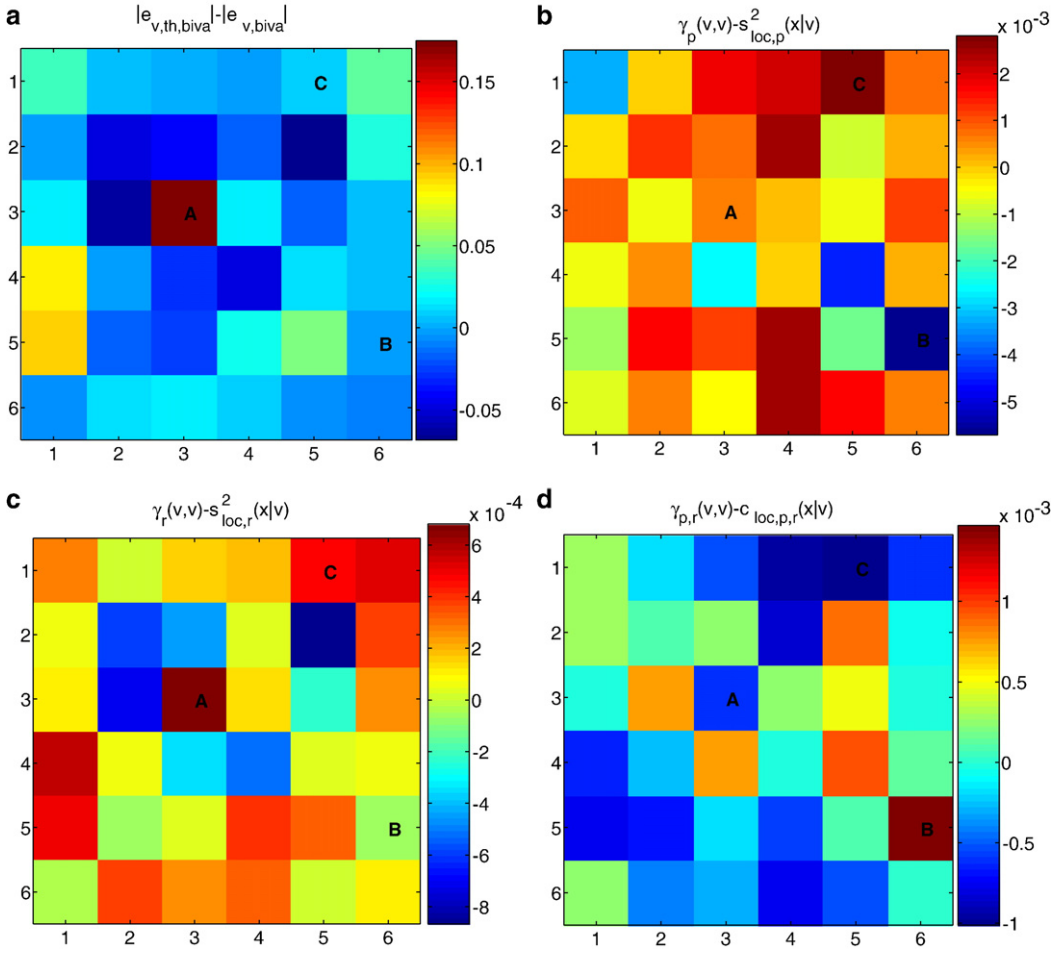

Fig. 11. Local estimation of the bivariate scaling bias over each 500 m moderate resolution pixel of the Alpilles01 scene. (a) Difference between the magnitude of the estimated scaling bias $|e_{v,\mathrm{biva,th}}|$ and the magnitude of the local bias $|e_{v,\mathrm{biva}}|$. (b) Difference between the theoretical dispersion variance $\gamma_p(v,v)$ and the local dispersion variance $s^2_{loc,p}(x|v)$ of the near infrared. (c) Difference between the theoretical dispersion variance $\gamma_r(v,v)$ and the local dispersion variance $s^2_{loc,r}(x|v)$ of the red. (d) Difference between the theoretical dispersion covariance $\gamma_{p,r}(v,v)$ and the local dispersion covariance $c_{loc,p,r}(x|v)$ between the near infrared and the red.

linearly explained by the relative scaling bias of the NDVI ($r^2=0.98$). If the NDVI scaling bias $e_{v,\mathrm{ndvi}}$ is negative (most of the Barrax03 pixels), it increases the negative LAI scaling bias e_v. But, when the NDVI scaling bias $e_{v,\mathrm{ndvi}}$ is positive (most of the Fundulea01 pixels), it compensates for the negative LAI scaling bias e_v.

This work illustrates how the scaling biases propagate through the composition of several non-linear models. They may compensate for one another or add up. This mechanism may be quantitatively important. For example, in the case under study, a relative scaling bias of 10% on the first function may decrease the scaling bias related to the second transfer function by 20%. This result confirms other studies such as Friedl (1997), who underlined that even a low bias related to LAI increases the scaling bias of the energy fluxes estimated from a non-linear function of LAI (transfer soil vegetation atmosphere model).

Finally, in practice, the estimation of LAI from the NDVI semi-empirical transfer function is achieved at moderate spatial resolution by using the $\mathrm{NDVI}_v^{\mathrm{app}}$ directly computed from the near infrared and red variables acquired at moderate spatial resolution. Therefore, it amounts to estimating the LAI from the bivariate transfer function $f_{p,r}$ of the near infrared and red variables (Eq. (16)). For most of the sites, because of the compensation effect with the NDVI scaling bias, the scaling bias caused by the non-linear relationship between NDVI and LAI is lower than the expected scaling bias due only to the non-linearity between LAI and NDVI.

5. Correcting the scaling bias

5.1. Univariate transfer function

The accuracy of the scaling bias correction is high on Alpilles01 at 1000 m spatial resolution with a RRMSE_{1000} of 0.8 (Fig. 7). However, it varies with the spatial resolution and from site to site (Fig. 8). For example, on Alpilles01, the correction is less accurate at 500 m spatial resolution ($\mathrm{RRMSE}_{500}=0.4$) than at 1000 m ($\mathrm{RRMSE}_{1000}=0.8$), because the local bias of one of the pixels is largely over estimated (pixel A in Fig. 9a). The over-estimation of the local spatial heterogeneity, $s^2_{loc}(x|v)$, by the dispersion variance $\gamma(v,v)$ (Fig. 9b) explains the failure of the model on this particular pixel. In addition, the significant degree of non-linearity associated with the high NDVI value of this pixel (Fig. 9c) amplifies multiplicatively the over-estimation of the bias. Conversely, on pixel C, although its local spatial heterogeneity is poorly quantified by $\gamma(v,v)$ (Fig. 9b), the bias is not over-estimated (Fig. 9a). The low degree of non-linearity of the transfer function related to the low NDVI value of the pixel C (Fig. 9c) prevents a large scaling bias. However, although the model may fail for a few 500 m moderate resolution pixels, on average, the accuracy of the correction over the whole image is very satisfactory.

The model relies on the second order stationarity hypothesis (Eq. (12)) which ensures that the variogram quantifies on average the local spatial heterogeneity of the moderate resolution pixels. The relevance of the second order stationarity hypothesis is verified if the variation of $s^2_{loc}(x|v)$ around $\gamma(v,v)$ is small. This depends strongly on the spatial resolution v. For most sites, $\gamma(v,v)$ represents better the local spatial heterogeneity at 1000 m spatial resolution than at other ones. The correction is thus the most accurate at 1000 m spatial resolution. Specially, on Fundulea01, the accuracy is very poor at pixel sizes smaller than 1000 m (Fig. 8), because on this site, the extent of the high spatial resolution image is not large enough with respect to the size of the field spatial structures. Consequently, the variogram does not provide an accurate quantification of the local spatial variability (Garrigues et al., 2006). For some sites such as Nezer01 or Puechabon01, the model is inaccurate for all moderate resolution pixels and for any of the spatial resolutions (Fig. 8). On these sites, the variogram does not reach a stationary sill at the image scale which implies that the second order stationarity hypothesis is not consistent with the data (Garrigues et al., 2006).

5.2. Bivariate transfer function

As displayed in Fig. 10, the bivariate model reduces the RMSE ($\mathrm{RRMSE}_{1000,biva}$ positive) on half of the sites at 1000 m spatial resolution (e.g. on Alpilles01 $\mathrm{RRMSE}_{1000,biva}=0.9$). The model accuracy varies also with the site and the spatial resolution (on Alpilles01 $\mathrm{RRMSE}_{500,biva}=0.2$). The failure of the model to estimate the scaling bias for some pixels is similarly due to a poor representation of the local dispersion variances and covariance of the red and near infrared variables by the direct variograms and the cross variogram of these high spatial resolution radiometric variables.

However, a poor correction of the scaling bias is more difficult to interpret than for the univariate case, because three sources of discrepancy between local and theoretical values of the dispersion variances and covariance may compensate for one another or add up (Eq. (21)). On Alpilles01, the over-estimation of the local scaling bias of pixel A (Fig. 11a) is caused by an over-estimation of the red local dispersion variance (Fig. 11c). But on pixel C, the over-estimation of the near infrared local dispersion variance (Fig. 11b) is compensated for by an under-estimation of the local dispersion covariance between the near infrared and red variables (Fig. 11d), leading to a small difference between the theoretical scaling bias and its local value (Fig. 11a).

The accuracy of the bivariate model is generally lower than that of the univariate model. On some sites or at some spatial resolutions, the model fails to estimate the scaling bias for all the moderate resolution pixels of the image (negative value of $\mathrm{RRMSE}_{v,biva}$). As with the univariate model, the bivariate model relies on the second order stationarity hypothesis. This hypothesis depends not only on the spatial resolution but also on the nature of the variable. Since it must be relevant for both near infrared and red variables, the estimation of the bivariate scaling bias is thus more constraining than in the univariate case.

6. Conclusion

This study provides a model to correct the scaling bias generated by non-linear estimation processes of LAI from

heterogeneous remote sensing data at moderate spatial resolution. The model is built first for a semi-empirical transfer function relating LAI to NDVI. The scaling bias is estimated on each moderate resolution pixel as a function of (i) the degree of non-linearity of the transfer function quantified by its second derivative and (ii) the intra-pixel spatial heterogeneity quantified on average by the variogram of the high spatial resolution (20 m) NDVI image. Then, the model is extended to a bivariate transfer function where LAI is related to the red and near infrared reflectances. The scaling bias depends on (i) the Hessian matrix of the transfer function and (ii) the variograms and the cross variogram of the high spatial resolution red and near infrared reflectances.

The magnitude of the scaling bias is evaluated on several distinct landscapes from the VALERI database. It increases rapidly with pixel size until the pixel is larger than the typical spatial scale of the data. Adjusting for scaling bias is generally critical on crop sites which are the most heterogeneous sites at the landscape level (LAI relative bias between 10% and 19% at 1000 m spatial resolution for the transfer function directly relating NDVI to LAI). Since natural vegetation and forest sites are more homogeneous than crop sites at the landscape level, the magnitude of their scaling bias is lower (LAI relative bias between 0.5% and 3% at 1000 m spatial resolution).

Since the NDVI is a non-linear function of the near infrared and red reflectances, we show that the scaling bias related to LAI is different when the transfer function is applied to the NDVI directly aggregated at moderate resolution than when it is applied to the NDVI computed from the aggregated near infrared and red reflectances. The scaling bias caused by the non-linearity of the NDVI as a function of near infrared and red reflectances adds up or compensates for the scaling bias between LAI and NDVI. In practice, LAI is estimated at moderate resolution from the NDVI computed from the near infrared and red reflectances acquired at moderate spatial resolution. In this case, for most of the sites, the scaling bias is lower than the expected scaling bias due only to the non-linearity between LAI and NDVI. This example illustrates how the scaling bias propagates through the composition of several non-linear models. Even a small bias related to the input variable of a non-linear model may increase dramatically the scaling bias of the model. Since estimation processes of land surface variables often result from the composition of several non-linear models, it is critical to account for this mechanism to improve the description of land surface processes.

Finally, the accuracy of the scaling bias correction depends mainly on the ability of the variograms and cross variogram to represent on average the local dispersion variances and covariance within a moderate resolution pixel. Results are generally better at 1000 m spatial resolution than at other ones. When the extent of the high spatial resolution image is large enough compared to the size of the image spatial structures, the information provided by the variogram is sufficient to quantify the mean spatial heterogeneity of the moderate resolution pixels. It is the case for most of the heterogeneous cropland sites studied in this work. On some landscapes for which the model is inaccurate, a larger image size would be more appropriate to better quantify the spatial heterogeneity. However, note that most of these sites are homogeneous at the landscape level and their scaling bias is thus negligible. Since the correction model is more constraining for the bivariate transfer function than for the univariate transfer function, the estimation of the scaling bias over the sites under study is generally less accurate for the bivariate transfer function.

In this approach, the variogram of high spatial resolution radiometric data is used as a proxy for the intra-pixel spatial heterogeneity. Its availability is critical to use this approach operationally to correct the scaling bias at moderate resolution. Therefore, way have to be found to get prior knowledge of this intra-pixel spatial heterogeneity metric without systematic concurrent high spatial resolution images that would make moderate resolution images useless. The variogram depends on two components: the spatial structure and the spatial variability of the data. These components can be retrieved by using either a temporal sampling or a spatial sampling per type of landscape of the high spatial resolution data. Further studies are required to test the effectiveness of this approach.

Acknowledgments

This study was mainly completed under a PhD grant allocated to the first author by the French Space Agency CNES (Toulouse, France) and Alcatel Space Industry (Cannes, France). It benefited also from the availability of the VALERI database under the responsibility of INRA Avignon (France) with funding mainly coming from CNES. Some writing of this work was sponsored by NASA Grant EOS/03-0408-0637, with thanks to the Program Manager Dr. Wickland.

References

Asner, G. P., & Townsend, A. R. (2000). Satellite observation of El Niño effects on Amazon forest phenology and productivity. *Geophysical Research Letters*, *27*(7), 981−984.

Avissar, R., & Chen, F. (1993). Development and analysis of prognostic equations for mesoscale (subgrid scale) fluxes for large-scale atmospheric models. *Journal of Atmospheric Sciences*, *50*(22), 3751−3774.

Baret, F., & Guyot, G. (1991). Potentials and limits of vegetation indices for LAI and FAPAR assessment. *Remote Sensing of Environment*, *35*, 161−173.

Baret, F., Weiss, M., Allard, D., Garrigues, S., Leroy, M., Jeanjean, H., et al. (accepted). VALERI: a network of sites and a methodology for the validation of medium spatial resolution land satellite product. *Remote Sensing of Environment.*

Cayrol, P., Kergoat, L., Moulin, S., Dedieu, G., & Chehbouni, A. (2000). Calibrating a coupled SVAT-vegetation growth model with remotely sensed reflectance and surface temperature a case study for the Hapex-Sahel grassland sites. *Journal of Applied Meteorology*, *39*(12), 2452−2472.

Chen, J. (1999). Spatial scaling of a remotely sensed surface parameter by contexture. *Remote Sensing of Environment*, *69*, 30−42.

Chen, J. M., & Black, T. A. (1992). Defining leaf area index for non-flat leaves. *Plant Cell Environment*, *15*, 421−429.

Chilès, J. -P., & Delfiner, P. (1999). *Geostatistics: Modeling spatial uncertainty.* New-York: Wiley Inter-Science, 695 pp.

Dungan, J. L. (2002). Toward a comprehensive view of uncertainty in remote sensing. In G. M. Foody, & P. M. Atkinson (Eds.), *Uncertainty in remote sensing and GIS* (pp. 25−33). New York: John Wiley and Sons.

Faivre, R., & Fischer, A. (1997). Predicting crop reflectances using satellite data observing mixed pixels. *Journal of Agricultural, Biological, and Environment Statistics*, *2*(1), 87−107.

Friedl, M. A. (1997). Examining the effects of sensor resolution and sub-pixel heterogeneity on spectral vegetation indices: Implications for biophysical

modeling. In D. A. Quattrochi, & M. F. Goodchild (Eds.), *Scale in remote sensing and GIS* (pp. 113−140). Boca Raton, USA: Lewis Publishers.

Friedl, M. A., Davis, F. W., Michaelsen, J., & Moritz, M. A. (1995). Scaling and uncertainty in the relationship between the NDVI and land surface biophysical variables: An analysis using scene simulation model and data from FIFE. *Remote Sensing of Environment*, *54*, 233−246.

Garrigues, S., Allard, D., Baret, F., & Weiss, M. (2006). Quantifying spatial heterogeneity at the landscape scale using variogram models. *Remote Sensing of Environment*, *103*, 81−96.

Hall, F. G., Huemmrich, K. F., Goetz, S. J., Sellers, P. J., & Nickeson, J. E. (1992). Satellite remote sensing of surface energy balance: success, failure, and unresolved issues in FIFE. *Journal of Geophysical Research*, *97*(D17), 19061−19089.

Heuvelink, G. B. M., & Pebesma, E. J. (1999). Spatial aggregation and soil process modelling. *Geoderma*, *89*, 47−65.

Houghton, J. T., Ding, Y., Griggs, D. J., Noguer, M., Van der Linden, P. J., & Xiaosu, D. (2001). *Contribution of Working Group I to the Third Assessment Report of the Intergovernmental Panel on Climate Change (IPCC).* Cambridge, UK: Cambridge University Press, 944 pp.

Hu, Z., & Islam, S. (1997). A framework for analyzing and designing scale invariant remote sensing algorithms. *IEEE Transactions on Geoscience and Remote Sensing*, *35*, 747−755.

Lovejoy, S., Schertzer, D., Tessier, Y., & Gaonac'h, H. (2001). Multifractals and resolution-independent remote sensing algorithms: The example of ocean colour. *International Journal of Remote Sensing*, *22*(7), 1191−1234.

Marceau, D. J., Gratton, D. J., Fournier, R. A., & Fortin, J. -P. (1994). Remote sensing and the measurement of geographical entities in a forested environment: 2. The optimal spatial resolution. *Remote Sensing of Environment*, *49*, 105−117.

Morisette, J. T., Baret, F., Privette, J. L., Myneni, R. B., Nickeson, J., Garrigues, S., et al. (2006). Validation of global moderate-resolution LAI Products: a framework proposed within the CEOS Land Product Validation subgroup. *IEEE Transactions on Geoscience and Remote Sensing*, *44*(7), 1804−1817.

Morisette, J. T., Privette, J. L., & Justice, C. O. (2002). A framework for the validation of MODIS land products. *Remote Sensing of Environment*, *83*(1–2), 77−96.

Moulin, S., Bondeau, A., & Delécolle, R. (1998). Combining agricultural crop models and satellite observations: From field to regional scales. *International Journal of Remote Sensing*, *19*(6), 1021−1036.

Myneni, R. B., Hall, F. G., Sellers, P. J., & Marshak, A. L. (1995). The interpretation of spectral vegetation indices. *IEEE Transactions on Geoscience and Remote Sensing*, *33*, 481−486.

Myneni, R., Nemani, R., & Running, S. (1997). Algorithm for the estimation of global land cover, LAI and FPAR based on radiative transfer models. *IEEE Transactions on Geoscience and Remote Sensing*, *35*, 1380−1393.

Pelgrum, H. (2000). Spatial Aggregation of Land Surface Characteristics. PhD thesis, Wageningen University, Netherlands, (150 p).

Raffy, A. M. (1994). Heterogeneity and change of scale in models of remote sensing-spatialization of multi-spectral models. *International Journal of Remote Sensing*, *15*, 2359−2380.

Running, S. W., Baldocchi, D., Turner, D. P., Gower, S. T., Bakwin, P. S., & Hibbard, K. A. (1999). A global terrestrial monitoring network integrating tower fluxes, flask sampling, ecosystem modeling and EOS satellite data. *Remote Sensing of Environment*, *70*, 108−127.

Sellers, P. J. (1987). Canopy reflectance, photosynthesis and transpiration: II. The role of biophysics in the linearity of their interdependence. *Remote Sensing of Environment*, *21*, 143−183.

Tian, H., Melillo, J. M., Kicklighter, D. W., McGuire, A. D., Helfrich, J. V. K., Moore, B., et al. (1998). Effect of interannual climate variability on carbon storage in Amazonian ecosystems. *Nature*, *396*, 664−667.

Tian, Y., Woodcock, C. E., Wang, Y., Privette, J. L., Shabanov, N. V., Zhou, L., et al. (2002). Multiscale analysis and validation of the MODIS LAI product: I. Uncertainty assessment. *Remote Sensing of Environment*, *83*, 414−430.

Townshend, J. R. G., & Justice, C. O. (1988). Selecting the spatial resolution of satellite sensors required for global monitoring of land transformations. *International Journal of Remote Sensing*, *9*, 187−236.

Verhoef, W. (1984). Light scattering by leaf layers with application to canopy reflectance modeling: the SAIL model. *Remote Sensing of Environment*, *16*, 125−141.

Wackernagel, H. (2003). *Multivariate geostatistics: An introduction with applications.* Berlin: Springer.

Weiss, M., & Baret, F. (1999). Evaluation of canopy biophysical variable retrieval performances from the accumulation of large swath satellite data. *Remote Sensing of Environment*, *70*, 293−306.

Weiss, M., Baret, F., Leroy, M., Hautecoeur, O., Bacour, C., Prevot, L., et al. (2002). Validation of neural net techniques to estimate canopy biophysical variables from remote sensing data. *Agronomie*, *22*, 547−553.

Weiss, M., Baret, F., Myneni, R. B., Pragnère, A., & Knyazikhin, Y. (2000). Investigation of a model inversion technique to estimate canopy biophysical variables from spectral and directional reflectance data. *Agronomie*, *20*, 3−22.